Soft Matter

PAPER

View Article Online
View Journal | View Issue

Cite this: *Soft Matter*, 2026, **22**, 3025

Glass transition and subphase anchoring govern the emergence of viscoelasticity in polymer interfaces

Daniel Ashkenazi,[a] Stelios Alexandris,[bc] Jan Vermant,[d] Dimitris Vlassopoulos[bc] and Moshe Gottlieb *[a]

Determining the rheological properties and the interfacial structure–property relationships for complex fluid–fluid interfaces is crucial for understanding physiological systems, and for designing and engineering industrial processes. While it is well established that polymer–laden interfaces can exhibit viscoelastic properties, the relationship between polymer molecular characteristics and interfacial mechanical response remains insufficiently understood. In this work, we investigate the role of two fundamental polymer properties: dynamic flexibility as manifested by the glass transition temperature (T_g) and anchoring strength to the water subphase. We examine the relative importance of these two properties as they govern interfacial morphology and rheology. To this end, we systematically study six homopolymers – poly(dimethylsiloxane), poly(*n*-butyl acrylate), poly(methyl methacrylate), poly(*tert*-butyl methacrylate), poly(4-vinylphenol), and polystyrene, that span a range of T_g values and water subphase interaction strengths. Their interfacial behavior is characterized by Langmuir–Pockels trough isotherms, interfacial shear rheology, Brewster angle microscopy (BAM), and neutron reflectivity. Film thickness and homogeneity are evaluated. Our findings show two distinct interfacial regimes: polymers with T_g below room temperature exhibit a morphology composed of discrete globular domains. Quantitative analysis of film thickness shows large interfacial heterogeneity. Their Langmuir isotherms are fully reversible, showing no hysteresis nor relaxation upon compression. Interfacial rheology measurements yield no detectable shear moduli. In contrast, high-T_g polymers form 1–2 nm thick continuous interfacial films. Their isotherms display pronounced hysteresis, significant relaxation at high compression, and no recovery after the first compression. They exhibit measurable viscoelastic moduli, even at moderate surface concentrations below full coverage of the interface. Polystyrene, with no interfacial affinity, fails to form an interfacial film and thus produces inconsistent rheological footprint. Taken together, these results establish that the formation of a viscoelastic polymer interface requires both a glass transition temperature exceeding the operating temperature and some minimal level of interaction with the aqueous subphase.

Received 24th January 2026,
Accepted 31st March 2026

DOI: 10.1039/d6sm00064a

rsc.li/soft-matter-journal

Introduction

Complex liquid interfaces populated by polymer molecules exhibit a wide range of microstructural and mechanical properties. Insoluble homopolymers deposited at the water/air interface differ markedly in their ability to form Langmuir monolayers, and in their static and dynamic interfacial behavior. Elucidating the rheological and structural properties of these complex interfaces is crucial for the design and engineering of industrial processes and for the understanding of environmental, physiological, and biomedical systems.[1]

Systematic investigation of the static properties of synthetic polymers at the air/water interface was initiated by Crisp,[2,3] who conducted a comprehensive study of the surface pressure (SP) - surface concentration compression isotherms using Langmuir–Pockels (LP) trough. A broad range of polymeric materials incorporating amphiphilic characteristics along their chains, such as ester or ether linkages which act as anchoring points into the aqueous subphase, were examined. Based on molecular architecture, Crisp[2,3] classified polymers into four categories: amorphous soft polymers, amorphous tough polymers, semicrystalline polymers with weak anchoring groups, and semicrystalline polymers with strong anchoring groups.

[a] *Department of Chemical Engineering, Ben-Gurion University, Beer Sheva, Israel. E-mail: mosheg@bgu.ac.il*
[b] *Department of Materials Science & Engineering, University of Crete, Heraklion, GR-70013, Greece*
[c] *Institute of Electronic Structure and Laser, FORTH, Heraklion, GR-70013, Greece*
[d] *Department of Materials, ETH Zurich, CH-8093 Zurich, Switzerland*

Each class exhibited a characteristic compression isotherm.[3] He concluded that polymers with low glass transition temperature (T_g) and highly hydrophilic moieties form fluid, homogeneous monolayers with reversible isotherms, while polymers with higher T_g and weaker interaction with water tend to yield heterogeneous films, often forming discrete domains or collapsing irreversibly under compression.[3] The work of Crisp underscored that two key attributes of the polymer: T_g and hydrophobicity distinguished one type from the others and identified these two as equally responsible for determining the static properties (*i.e.*, compression isotherms) of the polymer laden water/air interface. In the following, we therefore refer to dynamic molecular flexibility and polymer–subphase interaction strength rather than T_g and hydrophobicity, respectively.

Following this first report, a large number of studies were carried out on the compression isotherms of select polymers such as polydimethylsiloxane (PDMS), poly (methyl methacrylate) (PMMA), poly (methyl acrylate) (PMA), and polystyrene (PS). The aim of these studies was to relate the observed features of the isotherms to the molecular conformation of the polymers at the interface. For example, different regions in the compression isotherm of PDMS were associated with caterpillar-like conformation in which the Si–O–Si bonds lie parallel to the interface. As compression increases, this conformation is succeeded by the formation of helices either parallel or normal to the interface, followed by pancake multilayers at high compressions.[4–13] The details regarding some of these conformations were inferred from spectroscopic measurements such as polarization modulated IR reflection[8] or vibrational sum frequency spectroscopy,[13] while others were based on neutron reflectivity (NR) studies.[9–12]

The compression isotherm obtained for isotactic PMMA (i-PMMA) exhibits a plateau in intermediate compression values that is not observed for atactic (a-PMMA) and syndiotactic PMMA (s-PMMA). Beredjick *et al.*[14] and Brinkhuis *et al.*[15] attributed the plateau to an extended molecular conformation at the interface. Conformational energy calculations carried out by Vacatello and Flory,[16] and Sundarajan[17] led to the conclusion that the dynamic flexibility of i-PMMA backbone ($T_g < 60\ ^\circ C$) relative to the two other PMMA species ($T_g > 120\ ^\circ C$) is responsible for this plateau since it allowed optimal orientation of polar groups toward the water subphase. Vibrational sum frequency and polarization modulated IR reflection spectroscopies allowed Hong *et al.*[18] to attribute the 'shallow' compression isotherms of PMA to moderate increase of the order of methyl groups in the ester side chain (s-CH3), as compression was increased. In contrast, it was speculated that a-PMMA chains formed compact globules even at low compression, with no change in the orientation of the methyl groups (s-CH3), resulting in a sharp increase in SP with compression.[18]

The high-T_g, hydrophobic PS, exemplifies the class of materials that Crisp suggested will fail to form continuous monolayers[2,3] as was confirmed by the transmission electron microscopy study of Kumaki.[19] Furthermore, the latter suggested that the measured SP arises not from reduction in surface tension, but rather from the mechanical stresses exerted on the measuring probe by the PS ''floating islands''.

While the Crisp classification[2,3] provides a useful framework for rationalizing the static interfacial behavior of polymer films, it offers limited insight into their dynamic and rheological properties. Despite extensive efforts to relate molecular conformation to compression isotherms, comparatively little attention has been paid to the mechanical response of polymer–laden interfaces under deformation. Yet, interfacial rheology and time dependent behavior (*e.g.*, SP relaxation, recovery after compression) are of primary importance in processes that involve flow and deformation of interfaces.[1,20]

Considerable uncertainty still exists concerning the interfacial shear rheological behavior of polymeric films. Langmuir films of glassy polymers (PMMA) were reported to show a strong dependence of the interfacial rheology on molecular weight (N^4 dependence of both shear moduli) when employing a bicone accessory.[21] No such dependence on molecular weight above modest polymer surface concentrations ($\sim$15–17 Å^2/monomer – the surface pressure plateau), was observed when the magnetic needle Interfacial Shear Rheometer has been used.[22]

Poly(*tert*-butyl methacrylate) (PtBMA), poly(*tert*-butyl acrylate) (PtBA), and poly(*n*-butyl acrylate) (PnBA), polymers with roughly similar groups anchoring the molecules to the water subphase exhibit very different time dependent behavior.[23–25] PDMS a highly flexible, low-T_g polymer which is characterized by an intricate and easily measurable compression isotherm defies rheological characterization of the interface. At the same time Maestro and coworkers[26,27] reported detailed interfacial viscosity measurements on PtBA, another flexible, relatively low-T_g polymer, albeit with three orders of magnitude difference between interfacial viscosity values obtained by macro- and microrheological methods. Furthermore, measurements of the rheology of these PtBA films served to argue for the existence of reptation and entanglements in two-dimensional Langmuir films. These results have been contested by Samaniuk and Vermant[25] who attributed the orders of magnitude disagreement in the rheological measurements to heterogeneities with characteristic length scales from tens to hundreds of micrometers in PtBA films in contrast to the good agreement between the macro- and microrheological measurements in PtBMA films. Thus, the molecular characteristics that govern the dynamic and rheological behavior of polymers at the interface require further investigation.

Although interfacial rheological measurements remain experimentally challenging,[28] recent methodological advances now enable more reliable characterization of polymer–laden interfaces.[29] In this work, we leverage these developments to systematically elucidate the relationships among compression–expansion isotherms, interfacial microstructure, and mechanical response. By judicious selection of polymers spanning a range of dynamic flexibilities and subphase interaction strengths, and by combining LP isotherms with Brewster angle microscopy, neutron reflectivity, and interfacial shear rheology using a trough-mounted double-wall-ring rheometer (DWRT)[28,29] will enable us to gain new insights into the roles

of the dynamic chain flexibility and polymer–subphase interactions on the resulting interfacial morphology and rheology.

Experimental

Materials

The characteristics of the homopolymers employed in this work are listed in Table 1 and the rationale for the selection is explained in Fig. 1. PtBMA, PS, and poly(4-vinylphenol) (P4VPh) were purchased from Sigma-Aldrich, PDMS was purchased from United Chemical Technologies (UCT), PnBA and poly(*n*-butyl methacrylate) (PnBMA) were purchased from Polymer Source, two samples of a-PMMA (55% atactic, 45% syndiotactic) differing in molar mass were purchased from Polymer Source (lower molar mass) and from Polymer Standard Service (higher molar mass). All polymers were used as received. Note that PDMS, PtBMA, and P4VPh have relatively higher polydispersity compared to the other polymers. To a first approach this is not considered to substantially change the properties discussed and polydispersity effects are not considered in this work.

To systematically investigate the relationship between polymer chain flexibility, anchoring strength, and interfacial behavior, we selected a representative set of homopolymers that span a wide range of T_g values and anchoring strength to the aqueous subphase, as illustrated in Fig. 1. The various possible types of interaction mechanisms between insoluble polymer molecules deposited on the water/air interface and the subphase may result in different levels of anchoring strength to the interface. These may include polar interactions, hydrogen bonding, partial solubility of amphiphilic entities, weak dispersion forces, or electrokinetic interactions.[30–32] Here we selected to assign $\Delta G_{adsorption}$, the free energy gain upon

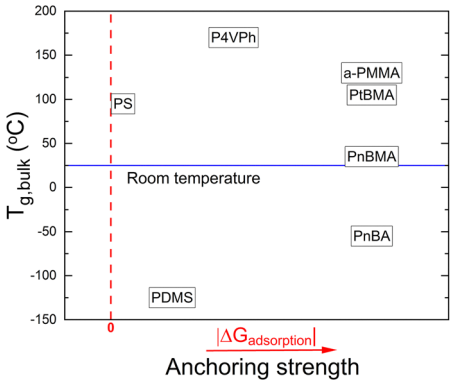

Fig. 1 A schematic illustration for the T_g and anchoring strength for the examined polymers.

Table 1 Homopolymers used in the current work. Molecular mass was determined by SEC using PS standards. Bulk T_g values were determined by DSC (midpoint, 5 deg min^{-1} heating/cooling rate). *D*-Number of repeat units. Refractive index values were obtained by Rudolph Scientific J257 automatic refractometer

Polymer designation	Bulk T_g (°C)	Mn (kg mol^{-1})	Polydispersity (PD)	Refractive index	Structural formula
PDMS (D1800)	−130 ± 5	133	2.5	1.40	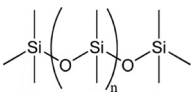
PDMS (D240)	−130 ± 5	18	2.4	1.40	
PnBA	−55 ± 3	77	1.18	1.47	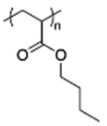
PnBMA	36 ± 1	150	1.5	1.51	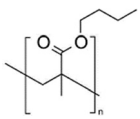
PtBMA	105 ± 3	76	1.8	1.46	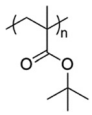
a-PMMA	120 ± 0.5	99	1.12	1.49	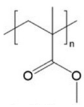
a-PMMA	130 ± 1	270	1.04	1.49	
PS	95 ± 5	55	1.01	1.59	
P4VPh	170 ± 5	10	1.8	1.60	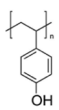

adsorption of a polymer segment onto the aqueous interface as an intuitive measure of the anchoring strength although its experimental quantification is not straightforward.

PDMS and PnBA are characterized by T_g significantly below room temperature (−125 °C and −55 °C, respectively) whereas a-PMMA, PtBMA, PS, and P4VPh are glassy polymers with T_g values above 90 °C. It should be noted that the three polyacrylates share the same polar acrylic side group which is expected to enhance their interaction with the aqueous subphase. It distinguishes them from PDMS, which features a weaker polar ether group in its backbone. PS and P4VPh are both high-T_g polymers exhibiting significant steric hindrance due to bulky aromatic side groups, that are expected to influence their packing and interfacial organization. P4VPh closely resembles PS, differing only by the presence of a phenol polar group on the aromatic side group. PS is devoid of any polar groups. The comparison between these structurally similar polymers will isolate the role of anchoring strength in modulating the interfacial behavior of high-T_g polymer chains.

Finally, PnBMA is a glassy acrylate polymer with bulk T_g ~10–15 °C above room temperature. We have used it to observe qualitative changes in film morphology upon heating from temperatures somewhat below T_g to temperatures above it.

It should be noted that T_g values of Langmuir films of glassy polymers are lower than their bulk values as revealed by the numerous studies over the last few decades focused on nanometric polymer films.[33] Although the large majority of these studies involved supported or free-standing films, the reduction in T_g observed in polymer films deposited on a liquid subphase was also addressed.[22c,34–38] The reduction in T_g values is attributed to a combination of faster molecular relaxation at the free surface,[36,38] plasticization by water absorbed from the subphase[39] or from ambient humidity,[40] and the dynamic heterogeneity related to density fluctuations.[41] The extent of reduction determined by different experimental methods varies: it is more pronounced for static thermodynamic measures such as thermal expansion than for dynamic measures such as molecular relaxation times.[42] Nevertheless, on the basis of all available data[33–42] T_g reduction is not expected to exceed 20–30 °C and since all measurements in this study were performed at room temperature, the high-T_g polymers are expected to remain in a glassy state at the interface.

All polymers were dissolved in chloroform purchased from Bio-Lab (purity > 99.9%). This solvent is a good solvent for all polymers tested here, it is weakly polar, very slightly miscible in water (8 g L^{-1}), denser than water (1.49 g cm^{-3}) and highly volatile (vapor pressure 200 mm Hg at room temperature, boiling point 61 °C at atmospheric pressure). In this work we have not considered the role of the solvent on polymer spreading (*e.g.*, effect of initial polymer conformation) but, as pointed out below, we verified it had no impact on interfacial properties. Before each measurement, a fresh highly diluted solution was prepared (concentrations between 0.10 to 0.30 ± 0.01 mg mL^{-1}, below the overlap concentration). Millipore purified deionized (DI) water, with an electrical resistance of 18.2 MW·cm was used as the aqueous subphase in all experiments.

Surface pressure measurements

Two different LP troughs were used for obtaining SP-area isotherms: KSV Nima mini trough (30 × 7.5 cm^2) and KSV Nima mini-extended trough (70 × 7.7 cm^2). Before each measurement, the trough and barriers were thoroughly cleaned by several DI water and ethanol wash cycles. The rectangular Platinum Wilhelmy plate (WP) (wetted perimeter 39.24 mm, height 9 mm, KSV Nima) was first cleansed by a propane burner's flame, followed by several ethanol and DI water wash cycles. The trough was filled with DI water, the Wilhelmy plate was positioned in the center of the trough, and the barriers were in their fully open position.

The cleanliness of the water surface was verified by compressing the pristine air–water interface. The interface was considered clean if the change in surface pressure upon full compression did not exceed 0.2 mN m^{-1}. Depending on the polymer type and the trough size, between 9 and 200 μL of the dilute polymer solution in chloroform were deposited dropwise at the interface by a 50 μL Hamilton glass micro syringe. The system was allowed to equilibrate for at least 15 minutes before measurements to allow evaporation of the solvent and even spreading the polymer at the interface. Preliminary tests indicated that the surface pressure of the clean water interface, as defined above, was fully recovered approximately 10 min after depositing 200 μL of chloroform. No thermostatic control of the trough was employed, room temperature was maintained at 23 ± 3 °C.

Compression/expansion isotherms. All compressions were carried out at 3 mm min^{-1} constant speed of the barriers. Subsequently, an expansion was carried out at the same barrier speed. At least three cycles of compression/expansion were performed. Data is reported in terms of the SP as function of the molecular area *i.e.*, nominal area occupied by a monomer. The latter values were determined by dividing the surface area between the trough barriers by the number of monomers deposited on the interface. These are nominal values which do not account for possible formation of stacked polymer layers or buckling at high compressions.

For viscoelastic interfaces above some critical polymer surface concentration, measurable differences in the SP are observed at different orientations of the WP relative to the barriers. These differences are due to the contribution of additional rheological stresses to the overall SP and may be used for qualitative evaluation of the rheological character of the interfacial film, as discussed in various studies.[43–45]

Relaxation isotherms. Material relaxation is a manifestation of viscoelastic behavior. Relaxation isotherms served as an additional method to obtain qualitative information on the interfacial rheological properties. Initially, the interface was compressed to the desired surface concentration. Then, while maintaining a constant interfacial area, the change in SP with time was monitored.

Brewster angle microscope (BAM)

The Nanofilm EP3 Ellipsometer (KSV-Nima, Biolin Scientific) was used for Brewster Angle Microscopy (BAM) imaging of the

polymer–laden interfaces. A *p*-polarized laser beam, incident on the subphase liquid at the Brewster angle, will not reflect from its surface. However, it will be reflected from the polymer film on top of it due to the differences in refractive indices between the subphase and the polymer. The reflected light goes through an analyzer to a CCD camera, which captures the reflected light and generates images with a spatial resolution of approximately two microns.

The polymer film thickness may be calculated from the grey level measured by the CCD camera as follows. The reflected light intensity of clean water at several angles of increasing deviation from the Brewster angle (up to $\pm 0.3^\circ$) is measured (in grey level units). The measured grey level is converted into reflected light intensity R_p, by applying the Fresnel equations for the water/air interface. This procedure allows conversion from grey level values to intensity values. Now, the film thickness l, can be calculated assuming a smooth and thin interface:[46]

$$l = \frac{\sqrt{R_p}}{\sin(2\theta_B - 90)} \frac{\lambda(n_1^2 - n_2^2)n_P^2}{\pi\sqrt{n_1^2 + n_2^2(n_1^2 - n_P^2)(n_2^2 - n_P^2)}} \quad (1)$$

where λ (=532 nm in the present configuration) is the incident wavelength, n is the refractive index (values used for the polymers are listed in Table 1), the subscripts 1,2 and P represent water, air, and polymer, respectively, θ_B is the Brewster angle (=53.15 ± 0.02 degrees as determined by calibration of clean water surface before each measurement). With the quantitative capability of the BAM, we can determine both the film thickness and the film's heterogeneity. BAM images and thickness measurements have been obtained at several compression values along the LP isotherms. The measured thickness values represent an average over an area of $200 \times 150\ \mu m^2$ collected over approximately 0.15 s. Data were collected from approximately 10 000 measurements over a period of 30 minutes to provide reliable statistical analysis. The degree of surface coverage can be estimated as well from the fraction of zero thickness readings although these values are not reported here.

Neutron reflectivity (NR)

Neutron reflectivity measurements were performed at the air–water interface, using the AMOR reflectometer of the Swiss spallation neutron source (SINQ) at the Paul Scherrer institute (PSI) in Switzerland. In all experiments, the subphase consisted of deuterated water (D_2O), and an LP trough was used for the measurements at different SP values. Three incident angles (θ = 0.6°, 1.4°, and 2.4°), which gave a range of momentum transfer Q values ($Q = 4\pi \sin\theta/\lambda$, with λ being the wavelength) from about 0.1 to 1.5 nm^{-1} were used. The width of the neutron beam used was 50 mm and the footprint length was 92 mm (4.6×10^3 mm^2 illuminated interfacial area to be contrasted with 3×10^{-2} mm^2 in the BAM). Further information on the setup is provided elsewhere.[47,48] The dispersion method of polymer samples at the D_2O/air interface was identical to the one described for LP isotherms above.

Fitting procedure and data analysis. To fit the NR data, it was assumed that the polymer layer is uniform and characterized by a constant scattering length density (SLD), ρ. The SLD of a material, in the absence of absorption, is $\rho = N_A\Sigma(\delta_j/A_j)b_j$ where N_A is Avogadro's number, δ_j, A_j, and b_j, are respectively the mass density, atomic mass, and coherent scattering length of atom j. The SLD of PDMS and PMMA were calculated using the NIST SLD calculator (https://www.ncnr.nist.gov/resources/sldcalc.html). The density of the interfacial polymer layer is assumed to be the same as the bulk density of the polymer (0.965 and 1.15 g cm^{-3} for PDMS ana a-PMMA respectively). Therefore, the calculated SLD is 6.3×10^{-8} $Å^2$ for PDMS and 1.1×10^{-6} $Å^{-2}$ for a-PMMA. For background subtraction, we have used the constant value of 7×10^{-6} $Å^2$, which corresponds to the incoherent signal of deuterium at high Q. For a multiple layer model, the SLD profile normal to the surface is given by the following relation:

$$\rho(z) = \sum_{i=0}^{n}\left[\left(\frac{\rho_i - \rho_{i+1}}{2}\right)\left(1 - \mathrm{erf}\frac{z - z_i}{\sqrt{2}\sigma_i}\right)\right] \quad (2)$$

here z is the distance normal to the interface and σ_i the roughness of the interface between layer i and $i + 1$. The indices 0, 1, 2 correspond to air, polymer, and water respectively. The thickness of the layer is given by $d_i = z_i - z_{i+1}$. For air ($z = 0$) the SLD is $\rho_0 = 0$, and for D_2O it is $\rho_2 = 6.2 \times 10^{-6}$ $Å^{-2}$, as calculated using the NIST program available on the website specified above. The best-fit parameters were obtained by an iterative process of minimization of the difference between the experimental and calculated curves.[48]

Shear interfacial rheology

Oscillatory interfacial shear rheology was measured by means of a double wall ring (DWR) fixture mounted on an LP trough (DWRT). This setup enables the attainment of the desired surface concentration through the compression of a dilute solution and facilitates precise control of the SP throughout the entire experiment.[49,50] The advantage of employing this configuration, especially for glassy-polymer interfacial films, has been recently demonstrated.[29] The experimental apparatus consists of a specially designed Teflon cup with an inner radius of 14.25 mm and an outer radius of 22 mm, featuring two rectangular openings. This cup is positioned on an LP Ribbon trough, from Biolin Scientific. A 3D-printed ring made of Ti6Al4V alloy with an inner radius of 17 mm and an outer radius of 18 mm, equipped with three openings, is used, which, together with corresponding openings in the trough, allow uniform compression of the interface both inside and outside the ring, maintain a consistent interface on both sides of the geometry, and enable precise control of the SP during rheological experiments.

The experimental process involves a thorough cleaning of the trough and cup, followed by filling them with Milli-Q water. The ring is cleansed with ethanol and Milli-Q water and then dried before being affixed to a DHR-3 stress-controlled rheometer from TA instruments. Calibrations and corrections for

instrument inertia effects are carried out as detailed by Renggli *et al.*[28] The ring is gently lowered to the interface until the interface appears flat and well-defined. Subsequently, the polymer solution is carefully added to the interface. The system is then compressed to the desired concentration or SP and allowed to equilibrate for a minimum of 30 minutes (deemed sufficient based on the relaxation experiments described below). The entire procedure is repeated for each measured concentration using a fresh polymer sample. To ensure measurement accuracy, the surface pressure was continuously monitored to prevent drift during the experiments. So-called subphase corrections, to account for momentum diffusion towards the bulk, are carried out using an open-source Matlab code based on the algorithm described in the SI provided by Renggli *et al.*[28] The reproducibility and repeatability of these measurements was verified as described earlier.[29]

Results and discussion

In the following section, we will examine the relationship between the interfacial properties of the polymer–laden interfaces, the T_g value of the polymer, and the strength of anchoring to the subphase for the six selected polymers. Unless specified otherwise, the PDMS being examined is PDMS D1800 (Table 1). Fig. 2–4 provide a comparison of different aspects of LP isotherms, obtained for the six polymers. The interfacial rheological properties of these polymers are compared in Fig. 5 and the morphology data from BAM and NR, are provided in Fig. 6–9.

LP isotherms

Compression isotherms obtained with the WP oriented in parallel and perpendicular to the LP barriers are depicted for the six polymers in Fig. 2.

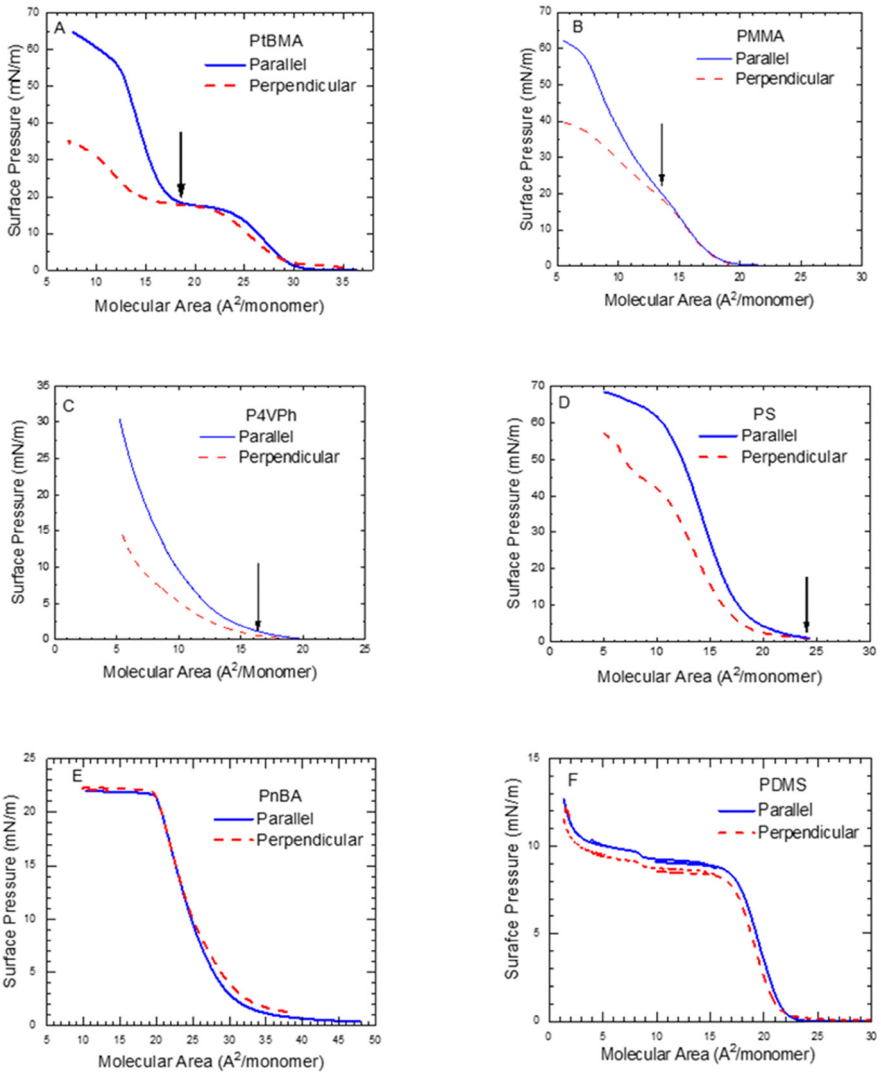

Fig. 2 Compression experiments with orthogonal orientations of the Wilhelmy plate for (A) PtBMA, (B) PMMA, (C) P4VPh, (D) PS, (E) PnBA, and (F) PDMS. The solid blue line represents compression with the WP parallel to the barriers, while the red dashed line represents compression with the WP oriented perpendicular to the barriers. Arrows indicate the point at which isotherms for the two WP orientations diverge. [Fig (A) and (B) have been reproduced from *J. Rheol.* 67(5), 1047–1060 (2023) with permission from the Society of Rheology (SOR)].

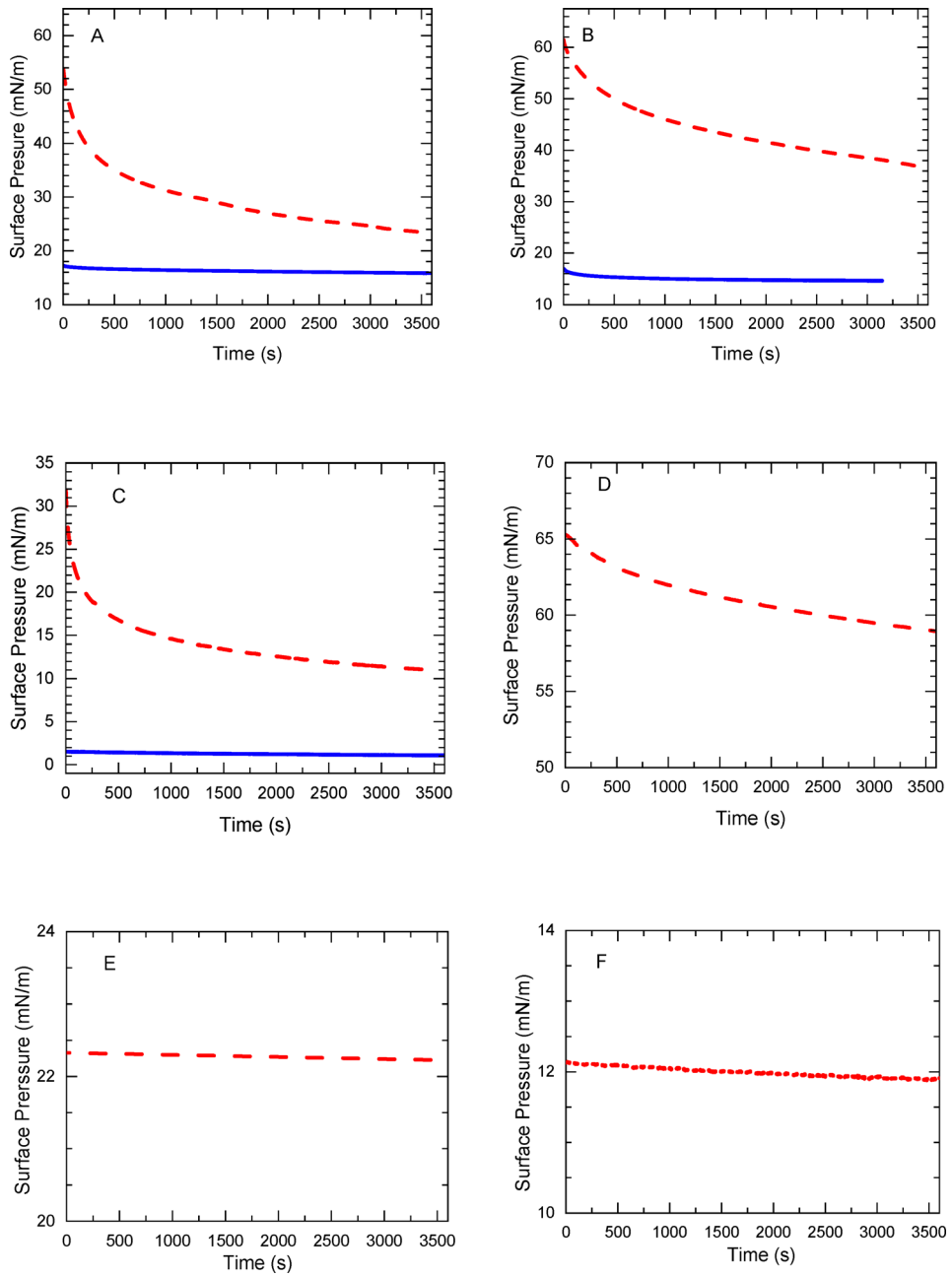

Fig. 3 Relaxation isotherms (change in SP with time at constant interfacial area) with the WP parallel to the barriers. Dashed line- relaxation following compression to high SP. Solid line- relaxation following compression to intermediate SP value. (A) PtBMA, the dashed line corresponds to 11 Å^2/monomer, the lower solid line corresponds to 22 Å^2/monomer. (B) PMMA, the dashed line corresponds to 5 Å^2/monomer, the solid line corresponds to 16 Å^2/monomer. (C) P4VPh, the upper dashed line corresponds to 5 Å^2/monomer, the solid line corresponds to 16 Å^2/monomer. For PS (D), PnBA (E) and PDMS (F), relaxation isotherms correspond to the highest compression achieved, 6 Å^2/monomer 10 Å^2/monomer and 0.8 Å^2/monomer, respectively.

The results show that for PtBMA and a-PMMA (Fig. 2A and B), an orientation dependent divergence between the isotherms obtained with the two Wilhelmy plate orientations emerges at molecular areas of approximately 18 and 13 Å^2/monomer, respectively.[29] In contrast, for P4VPh and PS (Fig. 2C and D), the divergence is apparent from the onset of the measurement, already in the gas-like regime at near-zero SP. No difference was observed between the isotherms obtained by the two WP orientations corresponding to PDMS or PnBA (Fig. 2E and F). As previously discussed, divergence between isotherms is indicative of the formation of an elastic, solid-like interface.[29,43–45] Therefore, the absence of any orientation dependent divergence for the isotherms of PDMS and PnBA suggests that these low-T_g polymers do not form solid-like interfaces within the examined range of surface concentrations. In contrast, PS and P4VPh exhibit solid-like interfacial behavior even at SP close to zero.

Another distinction between the high-T_g, dynamically rigid polymers and the low-T_g, flexible polymers lie in the surface SP

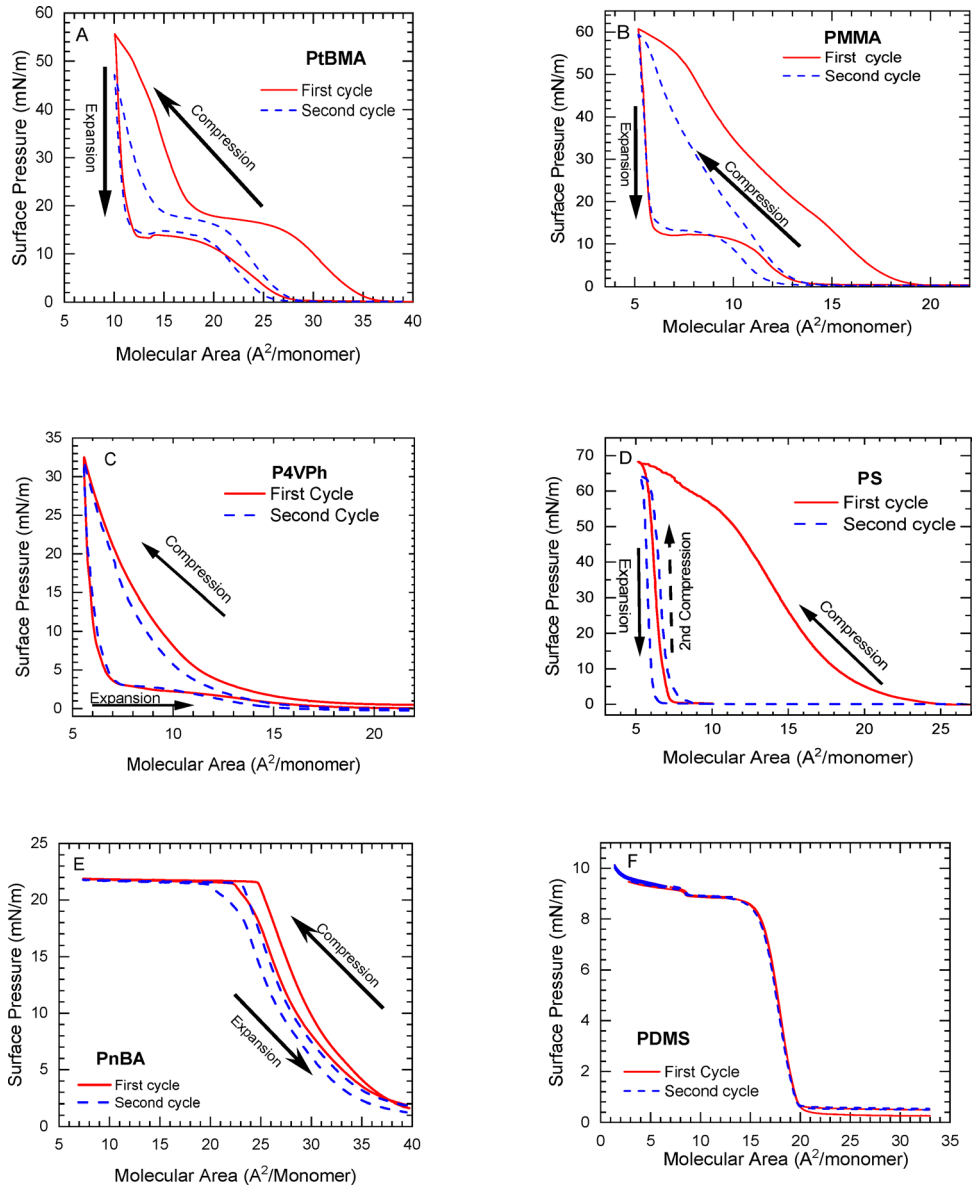

Fig. 4 Two compression–expansion cycles in the LP trough for (A) PtBMA, (B) PMMA, (C) P4VPh, (D) PS (E) PnBA and (F) PDMS.

values attained at maximum compression. The high-T_g polymers with the exception of P4VPh, exhibit SP values up to three times greater than those of PDMS and PnBA.

Next, we performed relaxation tests where the interfaces were compressed to the highest SP value obtained with the WP parallel to the barriers. The results from the first hour of relaxation are portrayed in Fig. 3. Three high-T_g polymers (PtBMA, PMMA, P4VPh) showed significant viscoelastic response, as inferred from a reduction of SP with time (dashed line in Fig. 3A–C). The other three polymers showed small ($<$10%) or no change in SP values over one hour (Fig. 3D–F). For the three polymers with significant relaxation at high SP values, an additional relaxation experiment was carried out following compression to an intermediate SP value, slightly lower than the value at the divergence point (solid line in Fig. 3A–C).

For PtBMA, PMMA, and P4VPh a decrease in the SP is observed only in the case of an elastic solid-like interface. At molecular area values smaller than the those at the divergence point (11 Å^2/monomer, for the first, 5 Å^2/monomer for the latter two), up to 50% reduction in SP is observed over the course of one hour. Conversely at surface concentrations below the divergence point (liquid interface), 22 Å^2/monomer for PtBMA and 16 Å^2/monomer for PMMA and P4VPh, the SP hardly changes during the experiment. No relaxation was observed for the low-T_g polymers PDMS and PnBA, measured at 0.8 and 10 Å^2/monomer, respectively (*i.e.*, the maximal attainable compressions).

Little relaxation ($\sim$10%) was observed for PS as well, despite its high T_g value. These results indicate that while the value of T_g is of major importance in determining the viscoelastic

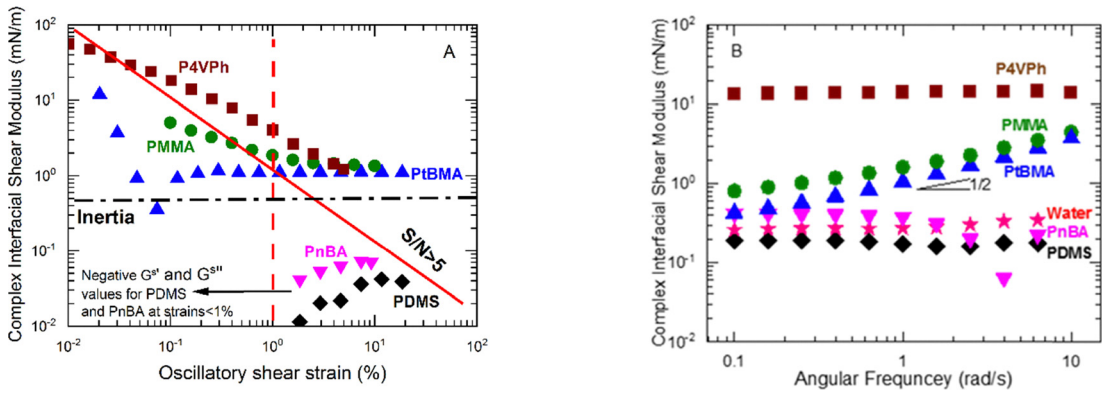

Fig. 5 (A) Magnitude of the complex interfacial shear modulus obtained by oscillatory strain amplitude sweeps at 1 rad s^{-1} by means of the DWRT. Values in (A) were corrected for subphase contribution. From top to bottom: P4VPh at 16 $Å^2$/monomer (squares), PMMA 14 $Å^2$/monomer (circles), PtBMA 22 $Å^2$/monomer (triangles), PnBA (inverted triangles), and PDMS (diamonds). The latter two at their highest compression (10 and 1 $Å^2$/monomer respectively). The diagonal solid line represents S/N = 5 determined as the lower limit of operation of DWRT at strain-controlled mode.[28] The black dashed horizontal line represents the instrument inertia contribution at 1 rad s^{-1}. The dashed vertical line marks 1% strain (below which both moduli values are negative for PnBA and PDMS). (B) Complex interfacial shear modulus obtained by frequency sweeps. Symbols same as in (A). Stars represent values for pristine water. The strain amplitudes were: P4VPh 0.03%, PMMA 3%, PtBMA, PDMS, PnBA and pristine water 1%. Values in (B) were not corrected for subphase contribution to allow direct comparison with data obtained for pristine water.

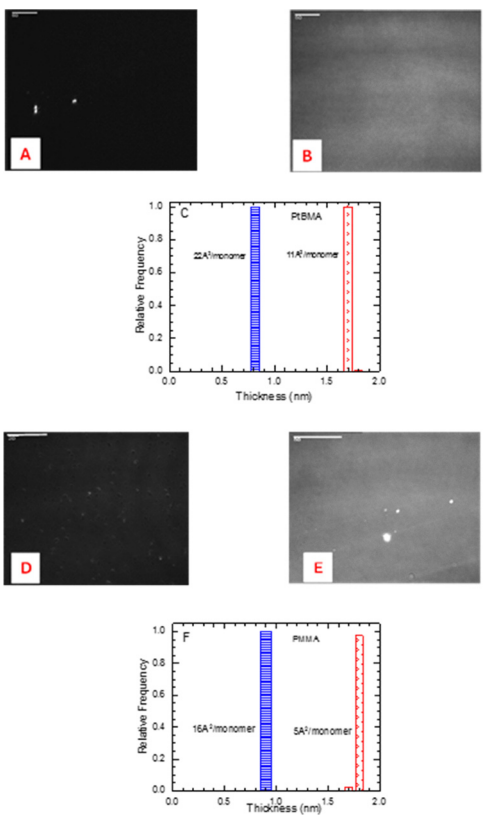

Fig. 6 BAM Images and film thickness distribution for PtBMA (A–C), and PMMA (D–F). Images A and D were obtained following deposition (no compression). Images B and E were obtained at the highest compressions. Scale bars (top left at each image) are 50 μm. The black background corresponds to the water subphase, grey level indicates a continuous layer over the water surface. Film thickness was determined at the surface concentration indicated.

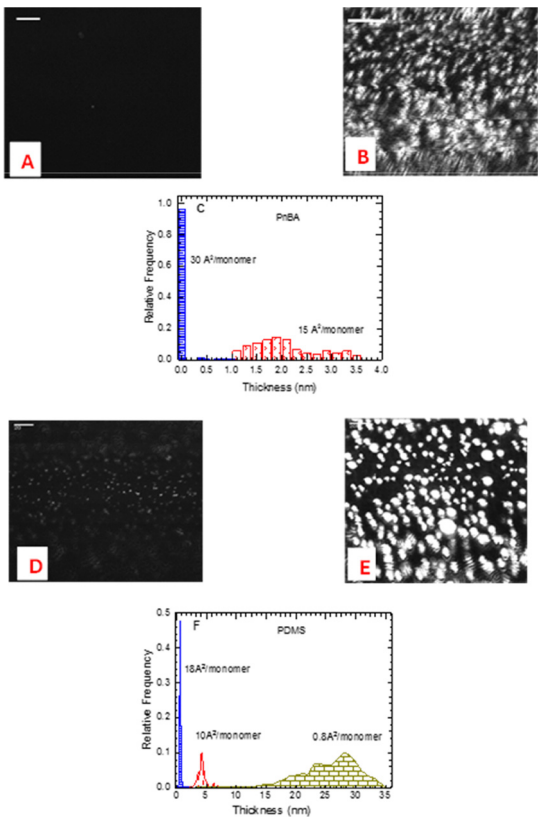

Fig. 7 BAM Images and film thickness distribution for PnBA (A–C), and PDMS (D–F). Images A and D were obtained following deposition (no compression). Images B and E were obtained at the highest compressions. Scale bars (top left at each image) are 20 μm. The black background corresponds to the water subphase, the brighter "spots" correspond to aggregates protruding from the interface. Film thickness was determined at the surface concentration indicated.

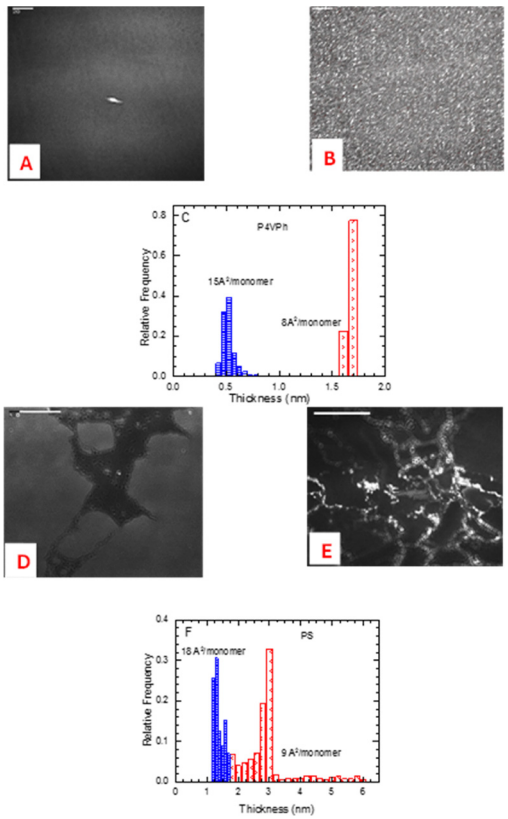

Fig. 8 BAM Images and film thickness distribution for P4VPh (A–C), and PS (D–F). Images A and D were obtained following deposition. Images B and E were obtained at the highest compressions. Scale bars (top left) are 20 μm for A and B and 100 mm for D and E. The black background corresponds to the water subphase, the brighter regions correspond to the polymer on top the interface. Film thickness was determined at the surface concentration indicated.

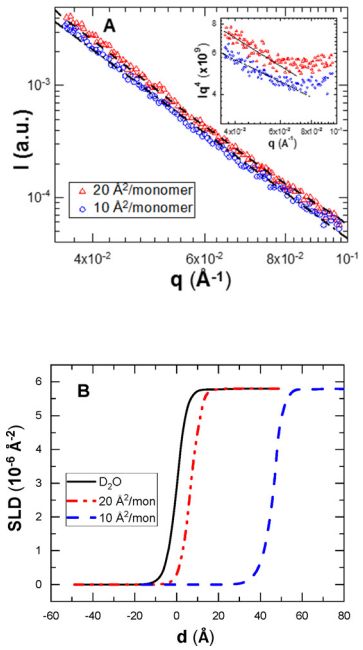

Fig. 9 (A) Neutron reflectivity curves of PDMS (D240) for surface concentrations of 20 Å^2/monomer (red triangles) and 10 Å^2/monomer (blue circles). Lines represent the fit to the data (B) Scattering length density profiles of D_2O (solid black line), 20 Å^2/monomer (dash-dot red line) and 10 Å^2/monomer (dashed blue line).

character of the polymeric layer at the interface, the appearance of a divergence in the compression isotherm as in the case of PS, does not necessarily imply the formation of an elastic film at the interface.

Next, several consecutive compression–expansion cycles were carried out with the WP positioned in the parallel orientation. The system was not allowed to relax between consecutive cycles. The resulting LP isotherms for the first two cycles are shown in Fig. 4 (the others were omitted for clarity). As can be observed, the isotherms for two high-T_g polymers PtBMA and PMMA (Fig. 4A and B) share many common features. These two polymers exhibit a large hysteresis between the compression and the consecutive expansion for both cycles presented. Immediately upon expansion, a sharp drop in SP is observed, a small undershoot, followed by a plateau, and a drop to zero SP at a surface concentration approximately 25% higher than the compression onset values. The onset of SP increase upon compression was observed at 35 Å^2/monomer for PtBMA and SP dropped to zero at 27 Å^2/monomer at the end of the expansion. For PMMA the onset of SP increase upon compression was observed at 20 Å^2/monomer and SP dropped to zero at 14 Å^2/monomer at the end of the expansion. The values at which the SP vanished upon the first expansion are similar to the values at which SP onset is observed in the second compression cycle. Additionally, the compression isotherm in this second compression step is considerably lower than the one obtained during the first compression over the entire range of surface concentrations.

The second expansion step follows quite closely the first expansion step in the initial sharp drop, undershoot, and plateau but lies below the first expansion curve in the final stage, and zero SP is obtained at yet slightly higher surface concentration. The third expansion/compression cycle (not shown for clarity) is almost identical to the second one hinting to an irreversible process that occurs during the first cycle and to a steady-state condition of the film in subsequent deformations.

In contrast, the low-T_g polymers PDMS and PnBA exhibit very different behavior (Fig. 4E and F). For PDMS, there is no discernible hysteresis between the compression and expansion processes, and complete recovery is achieved between successive cycles. Up to six cycles have been carried out with no difference between compression and expansion isotherms and between the different cycles. For PnBA, we observe only minor hysteresis, and as previously reported by Witte *et al.*,[51] a complete recovery between compression and expansion and between consecutive cycles is achieved.

The behavior of P4VPh (Fig. 4C) shares certain features with both the high-T_g and low-T_g polymers. On the one hand a sharp drop in SP is observed at the onset of expansion, followed by a plateau and a gradual decline to zero SP, resulting in a large

hysteresis between compression and expansion, like those exhibited by the high-T_g polymers. On the other hand, a complete recovery is observed at the end of the expansion, and the isotherms for the second cycle trace the ones for the first cycle, as for the two low-T_g polymers.

A unique pattern is observed for the case of PS: a sharp drop of the SP to nearly zero value is observed at the onset of expansion which defines the onset value for the second expansion cycle. In the first compression, the SP begins to increase at a molecular area of 22 Å^2/monomer, whereas in the second compression, this increase occurs at the value of 8 Å^2/monomer which is the endpoint of the first expansion. No hysteresis is detected in the second cycle and subsequent cycles trace back the second compression/expansion cycle.

The data depicted in Fig. 4 suggest that following full surface compression, interfaces laden with PDMS and PnBA can expand and trace back exactly their original SP and spatial distribution on the interface. In contrast, glassy polymers, such as PtBMA and PMMA, form glassy domains that may aggregate irreversibly upon compression or require long time (considerably longer than allotted during the expansion cycle at the temperature studied) to recover to the initial condition (individual molecules). The similarity of the LP isotherms of PnBA (Fig. 2–4) to those of PDMS rather than those of PtBMA and PMMA despite the similarity in chemical characteristics of the three polyacrylates indicates that the molecular dynamic flexibility as manifested by the glass transition temperature is more important than chemical affinity to the subphase in determining the compressional fingerprint of the polymer at the interface.

Both P4VPh and PS are high-T_g polymers. However, they exhibit distinctly different interfacial behaviors (Fig. 4C and D). While both systems undergo a sharp drop in SP at the end of compression, PS exhibits a brittle-like collapse characterized by an abrupt and nearly complete drop to zero SP. The SP isotherms for PS indicate a highly irreversible process, as reflected by the significant difference between the first and subsequent compression cycles. In contrast, although P4VPh demonstrates substantial yet repeatable hysteresis, the expansion endpoint is close to the compression onset value (unlike PMMA and PtBMA), and the second compression cycle for P4VPh closely follows the first expansion curve, indicating that the interfacial film exhibits elastic recovery. This difference is attributed to the presence of the hydrophilic hydroxyl groups in P4VPh, which facilitates interactions with the aqueous subphase. These results are entirely consistent with the BAM data discussed below.

Fig. 2–4 demonstrate that both the T_g and the interaction with the aqueous subphase play a role in determining the behavior of polymer films at the air–water interface. The comparison between PMMA, PtBMA, PnBA, and PDMS clearly indicates that T_g has a significant influence on the isotherm features such as the presence of a divergence (Fig. 2), relaxation (Fig. 3), and the hysteresis and recovery in consecutive compression–expansion cycles (Fig. 4). The comparison between P4VPh and PS further reveals that T_g alone does not fully account for the observed interfacial behavior. Despite their similarly high T_g values, P4VPh forms a recoverable film while PS exhibits an abrupt and irreversible collapse on expansion. These differences suggest that polymer–subphase interactions, contribute as well to layer stability and elasticity.

Interfacial shear rheology

Oscillatory shear experiments were carried out by means of the DWRT. Results for strain amplitude and frequency sweeps are presented in Fig. 5. Following Renggli *et al.*,[28] the operational window for reliable interfacial shear rheology, set by the signal-to-noise ratio and instrument inertia, was carefully verified in the present study. Although both storage and loss interfacial shear moduli were obtained, only interfacial complex modulus values are reported here to allow direct comparison to the analysis of Renggli *et al.*[28]

The upper limit of the operational window, which is considerably lower than the nominal upper torque specifications, is linked to the feedback loop employed when a stress-controlled rheometer is used in a strain-controlled mode (*e.g.*, TA DHR-3 used here). It is important to note that this upper limit is influenced by the mechanical properties and the physicochemical properties of the interface being studied.[52] Higher upper-limit values are allowed for highly elastic interfaces and lower values to more fluid interfaces.

The lower limit of the operational window is set by the rheometer's minimum torque sensitivity and by the ratio of the sample-induced torque to the instrument's inertial contribution. When inertial torques dominate, the signal-to-noise ratio decreases and measurement uncertainty increases. As shown by Renggli *et al.*[28] reliable measurements with the DWR geometry used here require S/N $>$ 5.

In Fig. 5A, we present a strain amplitude sweep conducted at 1 rad s^{-1} using the DHR-3 rheometer equipped with a double-wall ring (DWRT) and operating in strain-controlled mode. Corrections for subphase contributions were applied to all data, as detailed in the Experimental section above. The diagonal solid line represents the signal-to-noise threshold (S/N = 5), which defines the lower operational limit for reliable measurements of the DWR employed here under strain-controlled conditions as determined experimentally.[28] Data points located below this line are associated with low torque signals and as result are considered unreliable.

The horizontal dashed line marks the inertia limit of the instrument at this frequency. For data below this line, the contribution from instrument inertia becomes dominant and measured moduli values are unreliable. The high-T_g polymers PtBMA, PMMA, and P4VPh, were evaluated at relatively low surface concentrations (22, 14, and 16 Å^2/monomer, respectively), all in the liquid regime (below the divergence point indicated by the arrow in Fig. 2). P4VPh (squares) exhibits a pronounced strain softening response observed even at very low strain amplitudes. The magnitude of the complex modulus values of PMMA (circles) and PtBMA (triangles) are below the S/N threshold for stains smaller than approximately 1% while above the inertia limit for the presently utilized DWRT.

At higher strains they display largely linear viscoelastic behavior ($|G^*|$ independent of strain amplitude) up to approximately 20%, the highest value tested.

For PDMS and PnBA both at the highest possible compression, and over the entire range of strains above 1%, the moduli values remain significantly below the S/N operational limit, as well as below the inertia limit. At strains below 1%, the measured storage and loss moduli result in negative values.

Negative compressional surface viscosity values were reported for adsorbed layers of soluble surfactants. These anomalous values were obtained from the analysis of large frequency excited capillary waves characterized by large contribution from subphase inertia.[53] These apparent negative **compressional** viscosity values are unrelated to the negative **shear** moduli reported above for the insoluble polymeric layers of PDMS and PnBA at low frequencies, low strains ($<1\%$), and small subphase contribution. We maintain these negative values stem from instrumental limitations (low S/N, large instrument inertia contribution), are physically meaningless, and consequently are excluded from the figure.

No data is shown for PS, a glassy polymer with extremely weak anchoring to the water subphase since we were unable to obtain reliable interfacial shear measurements with the DWRT nor with the bicone or the Interfacial Shear Rheometer (ISR) (these latter two devices are described in detail elsewhere[28,29]). The most consistent results were obtained by using the ISR, but even here the results were untrustworthy. Two types of behavior were observed when visually tracking the magnetic needle of the ISR: either the needle remained immobilized regardless of the applied oscillatory magnetic force, or it moved freely across the interface even under minimal magnetic force. These two vastly different types of response observed for all surface concentrations, resulted in extremely poor reproducibility between repeated tests. These observations hint to the presence of ''particles'' or ''rafts'' of polymer molecules floating on top of the water interface as suggested by Kumaki[19] without interacting with the subphase. The needle either gets bogged down by colliding with these particles or moves freely when sampling only the water subphase. We conclude that the observed signals cannot be regarded as reflecting true properties of an interfacial viscoelastic film of PS, but rather mechanical forces applied by the probe on the ''rafts'' as suggested by Kumaki[19] in relation to the interpretation of PS compression isotherms.

Dynamic frequency sweep measurements were carried out at the same surface concentrations as in Fig. 5A and are depicted in Fig. 5B. Strain amplitudes were chosen individually for each polymer, based on the linear viscoelastic regime identified in Fig. 5A. The measurements were carried out at a strain amplitude of 0.03% for P4VPh, 3% for PMMA, and 1% for PtBMA, PnBA, PDMS, and pristine water. No correction for subphase contributions was applied for the data in Fig. 5B to be able to compare it to the data obtained for pristine water. The data clearly show that the three high-T_g polymers P4VPh, PMMA, and PtBMA exhibit measurable interfacial moduli revealing a viscoelastic response of the polymer–laden interface. In contrast, the low-T_g polymers PDMS and PnBA yield modulus values that are comparable to, or even lower than, those measured for pristine water, confirming the inability to measure interfacial viscoelasticity by the currently available interfacial rheometers.

PMMA and PtBMA display qualitatively similar viscoelastic liquid-like behavior over the examined frequency range - their complex interfacial shear moduli values increase with frequency such that $G^{S^*} \sim \omega^{1/2}$. In contrast, the complex shear modulus of P4VPh is independent of frequency and values are considerably higher than those displayed by PMMA and PtBMA.

From the interfacial shear rheology results above, we can speculate that the formation of a significantly viscoelastic interface requires a high T_g value. The presence of a polar group on the polymer chain capable of interacting with the water subphase is a necessary but insufficient requirement for the formation of rheological measurable viscoelastic interface. This can be inferred from the behavior of PS (no viscoelastic interface due to lack of interaction with the subphase) and PnBA (acrylate polar groups but low T_g). Additionally, different high-T_g polymers can exhibit distinct rheological characteristics. For example, P4VPh demonstrates a more gel-like (independent of frequency) response compared to the liquid-like behavior of PMMA and PtBMA. The difference could be attributed to the chemical or steric differences between the side chains (aromatic ring for the former and acrylate for the two latter), or stem from the more than 50 degrees higher T_g of P4VPh, or the ability to form $\pi-\pi$ stacking in contrast to hydrogen bridging. Further investigation is necessary to elucidate this point.

BAM imaging and neutron reflectivity

The influence of polymer characteristics on the morphology of the interfacial layer was assessed using Brewster angle microscopy (BAM). Interfacial film thickness distributions were obtained as histograms derived from the analysis of approximately 10 000 BAM images, and each BAM image reflects a signal averaged over a 200×150 μm^2 field of view. BAM images and film thickness distribution values at selected surface concentrations are provided in Fig. 6–8.

PtBMA and PMMA. The images depicted in Fig. 6 capture the morphological changes of the high-T_g PtBMA and PMMA laden interfaces upon compression and the accompanying film thickness histograms. At the gas phase (Fig. 6A and D for PtBMA and PMMA, respectively), a very small number of discrete globular white domains are visible against the dark background of the water subphase. Upon relatively modest compression to 22 Å^2/monomer (PtBMA, Fig. 6C) or 16 Å^2/monomer (PMMA, Fig. 6F), these domains vanish, and a 0.8 ± 0.05 or 0.9 ± 0.05 nm thick films for PtBMA and PMMA respectively, are formed. Upon further compression to considerably higher surface concentration values (11 Å^2/monomer and 5 Å^2/monomer for PtBMA and PMMA respectively) a homogeneous $1.7–1.8 \pm 0.1$ nm thick films of uniform thickness (Fig. 6C, and F) are observed. These highly compressed interfaces depicted in Fig. 6B and E, appear in the BAM images as motionless, frozen in time, featureless, homogeneous film of uniform grey level. The level of grey is a

measure of the elevation relative to the reference black water surface as expressed by eqn (1). These uniform grey images, and the accompanying thickness values are indications for the formation of continuous polymer monolayers. It should be noted that the BAM is limited to a planar resolution of 2–3 μm which doesn't allow detection of features such as nanometric perforations in the polymeric films.

As pointed out earlier, the carrier solvent used to initially introduce the glassy polymers onto the air–water interface impacts the homogeneity of the resulting film. As long as the rate of evaporation of the deposition solvent (chloroform in this case) is considerably faster than the rate of formation of glassy clusters, homogeneous films will be formed. When this was not the case, substantial heterogeneity in the polymeric layer was observed.[25]

PnBA and PDMS. The evolution of the interfaces laden with the low-T_g polymers PnBA and PDMS is presented in Fig. 7. For PnBA at low SP (Fig. 7A), no distinct features are visible. This is also manifested by the histogram at 30 Å^2/monomer (Fig. 7C) indicating the absence of any measurable thickness above the water surface. Upon compression to high SP (Fig. 7B), discrete bright spots appear, which are considerably smaller, with fuzzier borders, and more densely packed, than those observed for PDMS (discussed below in relation to Fig. 7E). These discrete polymeric domains have a broad distribution of thickness values between 0.8 and 4 nm with average around 2 nm (Fig. 7C).

In contrast, PDMS even at very low SP (surface concentration of 20 Å^2/monomer) exhibits large number of miniscule, elevated regions (0.7 nm thick bright spots in Fig. 7D) although 97% of the measurements are below the BAM resolution limit. Upon minor increase in surface concentration to 18 Å^2/monomer (Fig. 7F) 50% of the particles are large enough to be measured and these globular domains increase in number, size, and brightness. At 10 Å^2/monomer, the interface displays broadening of the thickness size distribution ranging from 2 to 6 nm, with an average of 4.5 ± 0.1 nm. At maximum compression (0.8 Å^2/monomer, Fig. 7E), the number of globules increases considerably, and the thickness distribution widens even further, ranging from 10 to 35 nm with an average thickness of 26 ± 0.5 nm. This 35-fold increase in average thickness upon compression serves as an indication to multilayer formation. The formation of multilayered PDMS "stacked pancakes" was also proposed by Kim *et al.*[13] based on their IR vibrational sum frequency spectroscopy results.

For the low-T_g polymers PnBA and PDMS the interface is composed of discrete, polydisperse "globules" unlike the uniform continuous films observed for PtBMA and PMMA. The images of the interfacial films for the high-T_g polymers depicted in Fig. 6 appear motionless ("frozen") in time. In contrast, the globules observed for the low-T_g polymers are in constant motion with particles entering and leaving the imaged area. The fuzzy appearance in Fig. 7B and somewhat less in 7E are attributed to this motion. While both PnBA and PDMS form non-uniform interfacial structures, the extent of multilayer buildup appears to be influenced by the strength of polymer–subphase interactions. The lower thickness observed for PnBA reflects a greater tendency of its chains to remain spread at the interface, whereas the more hydrophobic nature of PDMS and its weaker interaction with the water subphase promotes multilayer buildup upon compression.

P4VPh and PS. At low SP only few small, bright, elliptical domains are discernible on top of a 0.4–0.8 nm thick film of P4VPh (Fig. 8A and C) which gives way to a rugged 1.7 ± 0.1 nm thick film upon compression (Fig. 8B and C). The resulting film appears rougher in texture compared to PMMA and PtBMA.

On the other hand, PS (Fig. 8D–**F**), exhibits a very different interfacial morphology. At low SP (Fig. 8D), the interface is covered with irregular large bright domains, resembling floating rafts with thickness varying between 1.2 and 1.8 nm (Fig. 8F). As the compression proceeds (Fig. 8E and F), these domains become more prominent and exhibit signs of possibly, local buckling (white "ridges" in Fig. 8E) with thickness between 2 and 6 nm (Fig. 8F). No film is observed, and the interface coverage remains highly heterogeneous with water subphase (black) clearly visible between the highly elevated polymeric regions (grey and white).

Neutron reflectivity. To complement the thickness distribution measured with the BAM, the average layer thicknesses of PDMS D240 and PMMA were obtained through neutron reflectivity (NR) measurements. The NR data were analyzed using a one-layer fitting model with a uniform scattering length density across the interfacial film. Results for PDMS are presented in Fig. 9. A comparison between the thickness values obtained from BAM and those derived from NR is provided in Table 2. As noted previously, the NR measurements represent an average over a considerably larger illuminated area of 4.6 × 10^3 mm^2 which is five orders of magnitude larger than the area over which BAM measurements are averaged.

Initially, the neutron reflectivity data of the bare D_2O/air interface was analyzed. The best fit was obtained with SLD of D_2O of 5.8 × 10^{-6} Å^{-2} and surface roughness 4 Å (solid line in Fig. 9B). As pointed out above (*cf.* Section 2.4) NR analysis relied on the assumption of one-layer model with a constant SLD. By using eqn (2) and the procedure described above, the best fit to the reflectivity data resulted in PDMS film thickness of 7 Å and surface roughness of 1.2 Å at low compression (20 Å^2/monomer). Note that this surface roughness value is below BAM resolution. At the higher compression (10 Å^2/monomer) the thickness of the PDMS layer increased to 45.7 Å (dashed line Fig. 9B) with no change to surface roughness. NR measurements were obtained for PMMA at surface concentrations of 16

Table 2 Thickness of PDMS and PMMA interfacial layer from NR and BAM measurements

Polymer	Molecular area (Å^2/monomer)	Average thickness NR (nm)	Average thickness BAM (nm)
PDMS	20	0.7 ± 0.1	0.7 ± 0.1
PDMS	10	4.6 ± 0.1	4.5 ± 0.1
PMMA	16	1.0 ± 0.2	0.9 ± 0.1
PMMA	5	1.7 ± 0.2	1.8 ± 0.1

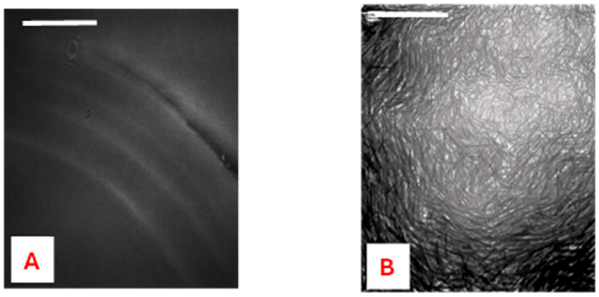

Fig. 10 BAM Images of PnBMA at 5 Å^2/monomer (A) at 22 °C ($T \cong T_{g,bulk} - 15$ °C) and (B) at elevated temperature ($T \approx 45$ °C, $\sim T_{g,bulk} + 10$ °C). Scale bars (top left) are 20 μm. The black background corresponds to the water subphase, grey level indicates a continuous layer over the water surface.

and 5 Å^2/monomer yielding film thickness values of 10 and 17 Å, respectively.

The good agreement between the thickness evaluation by the BAM and the NR, as summarized in Table 2, validates the accuracy of the quantitative determination of the layer thickness by the BAM method. The smaller area examined by the BAM affords better analysis of the film heterogeneity in comparison to the data obtained by the NR.

Taken together, these results highlight the relative roles of T_g and interfacial interactions in determining the morphology and thickness evolution of polymer films at the air–water interface. High-T_g polymers such as PMMA and PtBMA and P4VP consistently form upon compression homogeneous monolayer films, formed by compacted glassy domains anchored into the subphase by means of their polar groups. Yet, BAM images and thickness histograms for PS, indicate that a high T_g value alone is not sufficient to result in film formation. Rather, some degree of interaction between the polymer and the water subphase is needed. Low-T_g polymers, namely PnBA and PDMS, do not form macroscopically coherent films. Instead, their interfaces are composed of discrete, globular, weakly viscoelastic domains. Here as well, weaker interaction with the subphase results in stronger tendency for formation of multilayer stacked domains.

PnBMA. To further test whether a polymer interface adopts discrete globular domains at temperatures above T_g while it forms a continuous film at temperatures below T_g, we examined by BAM the interfaces formed by PnBMA, another polyacrylate with bulk T_g of 36 °C (somewhat lower for interfacial film as already discussed above). BAM images were acquired for PnBMA-laden interfaces at temperatures above and below T_g, allowing evaluation of the interfacial morphology of the same polymer on both sides of the glass transition. We were unable to measure the interfacial temperature directly. For temperature above T_g the circulation water bath was set to 75 °C resulting in 49 °C for the temperature of the water subphase near the interface and 32 °C for the air just above the interface. Although the estimated interfacial temperature was only moderately above the bulk T_g of PnBMA, it was the highest possible in the present configuration that allowed minimization of water evaporation required to maintain stable optical focus on the interface. For measurements below T_g no chiller was used and the water subphase and air temperatures in vicinity to the interface were both 22 °C. The BAM images depicted in Fig. 10 were acquired at a surface concentration of 5 Å^2/monomer; the corresponding isotherms are not shown.

Table 3 Summary of observations outlining the effect of T_g and the anchoring strength to the water subphase. High or low T_g are defined relative to room temperature

T_g	Characteristic	Strong anchoring	Modest anchoring	No anchoring
High	Interfacial morphology	• Uniform homogeneous film • Motionless frozen interface • Monolayer • No thickness distribution	• Rugged continuous film • Motionless frozen interface • Monolayer • Narrow thickness distribution	• No film, floating polymer rafts • Motionless frozen interface • Multilayer • Wide thickness distribution
	LB isotherms	• Dependance on WP orientation • Isotherms splits upon transition from liquid to elastic film • Relaxation • Hysteresis • No recovery after 1st cycle	• Dependence on WP orientation • Isotherms splits upon transition from liquid to elastic film • Relaxation • Hysteresis • Complete recovery after 1st cycle	• Dependence on WP orientation • Isotherms splits due to mechanical force on WP • Force and not SP is measured • Minor relaxation • Interface collapse after 1st cycle
	Interfacial shear rheology	Measurable shear viscoelasticity	Measurable shear viscoelasticity	Unmeasurable
Low	Interfacial morphology	• Discrete globules • No continuous film • Agitated motion of globules • Mono/bilayer • Narrow thickness distribution	• Discrete globules • No continuous film • Agitated motion of globules • Multilayer • Wide thickness distribution	
	LB isotherms	• Independent of WP orientation • No split of isotherms • No relaxation • Minor hysteresis • 1st & 2nd cycles identical	• Independent of WP orientation • No split of isotherms • No relaxation • No hysteresis • 1st & 2nd cycles identical	
	Interfacial shear rheology	Too low S/N value, weak shear viscoelasticity	Too low S/N value, weak shear viscoelasticity	

At temperature below $T_{g,bulk}$ (Fig. 10A), the interface appears as a continuous film, with bright features spanning across the image. These features likely correspond to buckling of the polymer film under the high compression. At the elevated temperature (Fig. 10B), these buckling lines are no longer visible, transformed into a heterogenous interface punctuated with small discrete domains which possibly are the early stages of larger globular structures. Since T_g is not a discrete point on the temperature scale but rather a continuous slow transition in molecular dynamics, the morphological transition of the interface is not expected to appear as a sharp threshold but rather as an evolving transformation from a relatively uniform film to a set of discrete domains over a range of temperatures. Similar heterogeneity of the interface was observed for PtBA (bulk T_g 45–50 °C) as well, and suggested as the reason for the failure to obtain reliable particle-tracking microrheological data.[25] While the change in morphology observed in Fig. 10 is not as pronounced as that distinguishing high- and low-T_g polymers (Fig. 6 and 7), the differences between the two temperatures are consistent with the hypothesis that interfacial structure is governed by the polymer dynamic flexibility or T_g. Given that the elevated temperature was only moderately above the T_g of PnBMA, it is expected that further increase in temperature would lead to a greater presence of globular domains, similar to those observed for PDMS and PnBA (Fig. 7B and E). Overall, these images reinforce the broader conclusion that the T_g is the key parameter in determining whether a polymer forms a homogeneous interfacial film or discrete domains.

Conclusions

The objective of this work was to elucidate how the interfacial behavior of polymers deposited at the air–water interface is governed by two key molecular characteristics: dynamic flexibility, as reflected by the glass transition temperature (T_g), and the strength of interaction with the aqueous subphase. A summary of the main observations is provided in Table 3.

Brewster angle microscopy (BAM) analysis demonstrates that high-T_g polymers form continuous interfacial films upon compression through the compaction and coalescence of the glassy domains initially present at low surface concentrations. The resulting films are largely homogenous with thicknesses of few nanometers and exhibit measurable shear rheological properties. The orientation-dependent divergence of the compression isotherms, together with pronounced relaxation, hysteresis, and the absence of recovery upon compression–expansion cycles, are all consistent with the formation of a viscoelastic interfacial film. The latter two features further suggest a highly irreversible process such as film fracture, following the expansion of the compressed elastic interface formed by the glassy polymers.

In contrast, Low-T_g polymers form discrete globular domains or droplets that remain highly mobile at the water-air interface. Upon compression, both the number and thickness of these globules increase, leading to multilayered aggregates that remain dispersed even at the highest accessible surface concentrations. The absence of LP isotherm divergence, relaxation, and hysteresis, and the complete recovery following compression/expansion cycles are all consistent with the dispersed polymeric domains structure of the interface. The particulate morphology of the interface results in the rheometer probe (*e.g.*, the ring in the DWR or the ISR needle) primarily interacting with the water subphase, while the polymeric domains move freely on the interface away from the probe without applying measurable stress on it. As result, measurement of the shear rheology for low-T_g polymers with available instrumentation remains challenging.

The BAM images for PS a high T_g polymer with practically no anchoring to the water subphase, revealed formation of floating polymer rafts that buckle and form highly heterogenous objects upon compression. In this case neither the LP isotherms nor interfacial rheology represent true interfacial behavior and are the result of artifacts stemming from the mechanical interactions with PS floating particulates residing at the interface. The case of PS should serve as a cautionary example for possible pitfalls in the interpretation of interfacial measurements.

In summary, our results demonstrate that dynamic flexibility, as reflected by the glass transition temperature (T_g) is the primary factor governing interfacial morphology and, consequently, interfacial rheology. Yet, comparisons between the interfacial properties of the chemically similar PS and P4VPh indicate that formation of a homogeneous viscoelastic film at the interface requires some degree of anchoring to the subphase in addition to a high T_g value.

Author contributions

Daniel Ashkenazi: investigation, writing – original draft, Stelios Alexandris: investigation, Jan Vermant: resources, writing – review & editing, Dimitris Vlassopoulos: resources, writing – review & editing, Moshe Gottlieb: supervision, resources, writing – review & editing.

Conflicts of interest

There are no conflicts to declare to any of the authors.

Data availability

All data are available in the paper.

Acknowledgements

Partial support by the European Commission (Horizon2020-INFRAIA-2016-1, EUSMI Grant No. 731019 and EUSMI Grants E180800154 and E190700306) is gratefully acknowledged. Neutron Reflectivity experiments were afforded and funded by PSI AMOR/SINQ Experiment 20170231. Drs Antigoni Theodoratou, Daniele Parisi, Thomas Geue, Benjamin Thompson, and

Damien Renggli are gratefully acknowledged for their assistance and contribution to the NR experiments, and Dr Sofiya Kolusheva at the BGU IKI Institute for Nanoscale Science and Technology for her help in carrying out BAM imagery. D. A. and M. G. acknowledge the financial support and travel grants from the Jim Blum Fund for the BGU Chemical Engineering Water Technology Research Program. We thank Prof. Greg McKenna for helpful discussion.

Notes and references

1 N. Jaensson and J. Vermant, Tensiometry and rheology of complex interfaces, *Curr. Opin. Colloid Interface Sci.*, 2018, **37**, 136–150, DOI: 10.1016/j.cocis.2018.09.005.
2 D. J. Crisp, Surface films of polymers. Part I. Films of the fluid type, *J. Colloid Interface Sci.*, 1946, **1**(1), 49–70, DOI: 10.1016/0095-8522(46)90006-2.
3 D. J. Crisp, Surface films of polymers. Part II. Films of the coherent and semi-crystalline type, *J. Colloid Interface Sci.*, 1946, **1**(2), 161–184, DOI: 10.1016/0095-8522(46)90014-1.
4 V. Bergeron, P. Cooper, C. Fischer, J. Giermanska-Kahn, D. Langevin and A. Pouchelon, Polydimethylsiloxane (PDMS)-based antifoams, *Colloids Surf., A*, 1997, **122**(3), 103–120, DOI: 10.1016/S0927-7757(96)03774-0.
5 W. Noll, *Chemistry and Technology of Silicones*, Academic Press, New York, 1968, Ch. 6.
6 W. Noll, H. Steinbach and C. Sucker, Monolayers of polyorganosiloxanes on water, *J. Polym. Sci., Part C*, 1971, **34**, 123–139, DOI: 10.1002/polc.5070340114.
7 E. K. Mann, S. Hénon, D. Langevin and J. Meunier, Molecular layers of a polymer at the free water surface: Microscopy at the Brewster angle, *J. Phys. II France*, 1992, **2**(9), 1683–1704, DOI: 10.1051/jp2:1992228.
8 T. D. Hahn, S. L. Hsu and H. D. Stidham, Reflectance infrared spectroscopic analysis of polymers at the air−water interface. 4. microstructure of poly(dimethylsiloxane), *Macromolecules*, 1997, **30**(1), 87–92, DOI: 10.1021/ma9611228.
9 L. T. Lee, D. Langevin, E. K. Mann and B. Farnoux, Neutron reflectivity at liquid interfaces, *Phys. B*, 1994, **198**(1), 83–88, DOI: 10.1016/0921-4526(94)90133-3.
10 L. T. Lee, E. K. Mann, D. Langevin and B. Farnoux, Neutron reflectivity and ellipsometry studies of a polymer molecular layer spread on the water surface, *Langmuir*, 1991, **7**(12), 3076–3080, DOI: 10.1021/la00060a029.
11 E. K. Mann and D. Langevin, Poly(dimethylsiloxane) molecular layers at the surface of water and of aqueous surfactant solutions, *Langmuir*, 1991, **6**(7), 1112–1127, DOI: 10.1021/la00054a016.
12 L. T. Lee, E. K. Mann, O. Guiselin, D. Langevin, B. Farnoux and J. Penfold, Polymer-surfactant films at the air-water interface. 2. A neutron reflectivity study, *Macromolecules*, 1993, **26**(25), 7046–7052, DOI: 10.1021/ma00077a050.
13 C. Kim, M. C. Gurau, P. S. Cremer and H. Yu, Chain conformation of poly(dimethyl siloxane) at the air/water interface by sum frequency generation, *Langmuir*, 2008, **24**(18), 10155–10160, DOI: 10.1021/la800349q.
14 N. Beredjick, R. Ahlbeck, T. Kwei and H. Ries, Differentiation of stereoregular polymethyl methacrylates by the film-balance technique, *J. Polym. Sci.*, 1960, **46**(147), 268–270, DOI: 10.1002/pol.1960.1204614728.
15 R. H. G. Brinkhuis and A. J. Schouten, Thin-film behavior of poly(methyl methacrylates). 1. monolayers at the air-water interface, *Macromolecules*, 1991, **24**(7), 1487–1495, DOI: 10.1021/ma00007a009.
16 M. Vacatello and P. J. Flory, Conformational statistics of poly(methyl methacrylate), *Macromolecules*, 1986, **19**(2), 405–415, DOI: 10.1021/ma00156a030.
17 P. R. Sundararajan, Conformational analysis of poly(methyl methacrylate), *Macromolecules*, 1986, **19**(2), 415–421, DOI: 10.1021/ma00156a031.
18 Y. Hong, H. Zhou, W. Qian, B. Zuo and X. Wang, Impact of the α-Methyl Group (α-CH3) on the aggregation states and interfacial isotherms of poly(acrylates) monolayers at the water surface, *J. Phys. Chem. C*, 2017, **121**(36), 19816–19827, DOI: 10.1021/acs.jpcc.7b06051.
19 J. Kumaki, Monolayer of polystyrene monomolecular particles on a water surface studied by Langmuir-type film balance and transmission electron microscopy, *Macromolecules*, 1988, **21**(3), 749–755, DOI: 10.1021/ma00181a033.
20 M. Rodriguez-Hakim, L. Oblak and J. Vermant, Facile and robust production of ultrastable micrometer-sized foams, *ACS Eng. Au*, 2023, **3**(4), 235–248, DOI: 10.1021/acsengineeringau.3c00005.
21 A. Maestro, F. Ortega, F. Monroy, J. Krägel and R. Miller, Molecular weight dependence of the shear rheology of poly (methyl methacrylate) Langmuir films: A comparison between two different rheometry techniques, *Langmuir*, 2009, **25**(13), 7393–7400, DOI: 10.1021/la9003033.
22 (*a*) G. T. Gavranovic, J. M. Deutsch and G. G. Fuller, Two-dimensional melts: polymer chains at the air−water interface, *Macromolecules*, 2005, **38**(15), 6672–6679, DOI: 10.1021/ma050061n; (*b*) G. T. Gavranovic, M. M. Smith, W. Jeong, A. Y. Wong, R. M. Waymouth and G. G. Fuller, Effects of temperature and chemical modification on polymer Langmuir films, *J. Phys. Chem. B*, 2006, **110**(44), 22285–22290, DOI: 10.1021/jp063396v; (*c*) S. Shrivastava, D. Leiske, J. K. Basu and G. G. Fuller, Interfacial shear rheology of highly confined glassy polymers, *Soft Matter*, 2011, **7**(5), 1994–2000, DOI: 10.1039/c0sm00839g.
23 L. R. Arriaga, F. Monroy and D. Langevin, Influence of backbone rigidity on the surface rheology of acrylic Langmuir polymer films, *Soft Matter*, 2011, **7**(17), 7754–7760, DOI: 10.1039/c1sm05338h.
24 F. Monroy, L. R. Arriaga and D. Langevin, Langmuir polymer films: recent results and new perspectives, *Phys. Chem. Chem. Phys.*, 2012, **14**(42), 14450–14459, DOI: 10.1039/c2cp42454.
25 J. R. Samaniuk and J. Vermant, Micro and macrorheology at fluid–fluid interfaces, *Soft Matter*, 2014, **10**(36), 7023–7033, DOI: 10.1039/c4sm00646a.

26 A. Maestro, H. M. Hilles, F. Ortega, R. G. Rubio, D. Langevin and F. Monroy, Reptation in Langmuir polymer monolayers, *Soft Matter*, 2010, **6**(18), 4407–4412, DOI: 10.1039/c0sm00250j.
27 A. Maestro, L. J. Bonales, H. Ritacco, T. M. Fischer, R. G. Rubio and F. Ortega, Surface rheology: macro- and microrheology of poly(*tert*-butyl acrylate) monolayers, *Soft Matter*, 2011, **7**(17), 7761–7771, DOI: 10.1039/C1SM05225J.
28 D. Renggli, A. Alicke, R. H. Ewoldt and J. Vermant, Operating windows for oscillatory interfacial shear rheology, *J. Rheol.*, 2020, **64**(1), 141–160, DOI: 10.1122/1.5130620.
29 S. Alexandris, D. Ashkenazi, J. Vermant, D. Vlassopoulos and M. Gottlieb, Interfacial shear rheology of glassy polymers at liquid interfaces, *J. Rheol.*, 2023, **67**(5), 1047–1060, DOI: 10.1122/8.0000685.
30 J. K. Beattie, A. M. Djerdjev and G. G. Warr, The surface of neat water is basic, *Faraday Discuss.*, 2009, **141**, 31–39, DOI: 10.1039/b805266b.
31 S. Strazdaite, J. Versluis and H. J. Bakker, Water orientation at hydrophobic interfaces, *J. Chem. Phys.*, 2015, **143**(8), 084708, DOI: 10.1063/1.4929905.
32 N. Agmon, H. J. Bakker, R. K. Campen, R. H. Henchman, P. Pohl, S. Roke, M. Thämer and A. Hassanali, Proton and hydroxide ions in aqueous solutions, *Chem. Rev.*, 2016, **116**(13), 7642–7672, DOI: 10.1021/acs.chemrev.5b00736.
33 B. Li, S. Zhang, J. S. Andre and Z. Chen, Relaxation behavior of polymer thin films: Effects of free surface, buried interface, and geometrical confinement, *Prog. Polym. Sci.*, 2021, **120**, 101431, DOI: 10.1016/j.progpolymsci.2021.101431.
34 H. M. Hilles, F. Ortega, R. G. Rubio and F. Monroy, Long-Time Relaxation Dynamics of Langmuir Films of a Glass-Forming Polymer: Evidence of Glasslike Dynamics in Two Dimensions, *Phys. Rev. Lett.*, 2004, **92**(25), 255503, DOI: 10.1103/PhysRevLett.92.255503.
35 L. R. Arriaga, F. Monroy and D. Langevin, The polymer glass transition in nanometric films, *Euro. Phys. Lett.*, 2012, **98**(3), 38007, DOI: 10.1209/0295-5075/98/38007.
36 J. Wang and G. B. McKenna, Viscoelastic and glass transition properties of ultrathin polystyrene films by dewetting from liquid glycerol, *Macromolecules*, 2013, **46**(6), 2485–2495, DOI: 10.1021/ma400040j.
37 C. O. Klein, A. Theodoratou, P. A. Rühs, U. Jonas, B. Loppinet, M. Wilhelm, P. Fischer, J. Vermant and D. Vlassopoulos, Interfacial Fourier transform shear rheometry of complex fluid interfaces, *Rheol. Acta*, 2019, **58**(1), 29–45, DOI: 10.1007/s00397-018-01122-y.
38 H. Tian, J. Luo, Q. Tang, H. Zha, R. D. Priestley, W. Hu and B. Zuo, Intramolecular dynamic coupling slows surface relaxation of polymer glasses, *Nat. Commun.*, 2024, **15**, 6082, DOI: 10.1038/s41467-024-50398-7.
39 Y. Fujii, T. Nagamura and K. Tanaka, Relaxation behavior of poly(methyl methacrylate) at a water Interface, *J. Phys. Chem. B*, 2010, **114**(10), 3457–3460, DOI: 10.1021/jp909373g.
40 H. C. Kim, Y. H. Choi, W. Bu, M. Meron, B. Lin and Y.-Y. Won, Increased humidity can soften glassy Langmuir polymer films by two mechanisms: plasticization of the polymer material, and suppression of the evaporation cooling effect, *Phys. Chem. Chem. Phys.*, 2017, **19**(16), 10663, DOI: 10.1039/c7cp00785j.
41 S. Napolitano, Projecting dynamic heterogeneity into nanoconfinement: the enduring legacy of the Long–Lequeux model, *Eur. Phys. J. E*, 2025, **48**(10–12), 79, DOI: 10.1140/epje/s10189-025-00547-7.
42 S. Yadav and C. B. Roth, Perylene dye as a measure of dynamic free volume, fragility, and dynamic glass transition in thin polystyrene films, *Macromolecules*, 2026, **59**(5), 2894–2905, DOI: 10.1021/acs.macromol.5c03244.
43 K. Halperin, J. B. Ketterson and P. Dutta, A study of the mechanical behavior of surface monolayers using orthogonal Wilhelmy plates, *Langmuir*, 1989, **5**(1), 161–164, DOI: 10.1021/la00085a030.
44 J. T. Petkov, T. D. Gurkov, B. E. Campbell and R. P. Borwankar, Dilatational and shear elasticity of gel-like protein layers on air/water interface, *Langmuir*, 2000, **16**(8), 3703–3711, DOI: 10.1021/la991287k.
45 M. Pepicelli, T. Verwijlen, T. A. Tervoort and J. Vermant, Characterization and modelling of Langmuir interfaces with finite elasticity, *Soft Matter*, 2017, **13**(35), 5977–5990, DOI: 10.1039/c7sm01100h.
46 J. M. Pusterla, A. A. Malfatti-Gasperini, X. E. Puentes-Martinez, L. P. Cavalcanti and R. G. Oliveira, Refractive index and thickness determination in Langmuir monolayers of Myelin lipids, *Biochim. Biophys. Acta, Biomembr.*, 2017, **1859**(5), 924–930, DOI: 10.1016/j.bbamem.2017.02.005.
47 D. Clemens, P. Gross, P. Keller, N. Schlumpf and M. Konnecke, AMOR - the versatile reflectometer at SINQ, *Phys. B*, 2000, **276**, 140–141, DOI: 10.1016/S0921-4526(99)01386-1.
48 M. Gupta, T. Gutberlet, J. Stahn, P. Keller and D. Clemens, AMOR - the time-of-flight neutron reflectometer at SINQ/PSI, *Pramana*, 2004, **63**(1), 57–63.
49 E. Hermans and J. Vermant, Interfacial shear rheology of DPPC under physiologically relevant conditions, *Soft Matter*, 2014, **10**(1), 175–186, DOI: 10.1039/c3sm52091a.
50 S. Vandebril, A. Franck, G. G. Fuller, P. Moldenaers and J. Vermant, A double wall ring geometry for interfacial shear rheometry, *Rheol. Acta*, 2010, **49**(2), 131–144, DOI: 10.1007/s00397-009-0407-3.
51 K. N. Witte, S. Kewalramani, I. Kuzmenko, M. Sun and Y. Won, Formation and collapse of single-monomer-thick monolayers of Poly(*n*-butyl acrylate) at the air−water interface, *Macromolecules*, 2010, **43**(6), 2990–3003, DOI: 10.1021/ma901842q.
52 A. Alicke and J. Vermant, Yielding of model particle-laden interfaces in shear and compression, *Rheol. Acta*, 2025, **64**(9–10), 583–600, DOI: 10.1007/s00397-025-01524-9.
53 D. Langevin and F. Monroy, Marangoni stresses and surface compression rheology of surfactant solutions. Achievements and problems, *Adv. Colloid Interf. Sci.*, 2014, **206**, 141–149, DOI: 10.1016/j.cis.2014.01.006.